
State of the Art: Discrete Element Modeling

1.1. Introduction

As mentioned in the previous chapter, in conjunction with the accelerating progress in computer science and software technology, the final decades of the 20th Century have seen an explosion of powerful numerical methods which can be classified into discrete methods (DMs) and continuum methods (CMs). These methods have been used over the years to simulate a wide variety of mechanical problems at different scales. Typically, four scales can be distinguished in the context of numerical simulation:

- the nanoscopic (or atomic) scale ($\sim 10^{-9}$ m), where phenomena related to the behavior of electrons become significant. At this scale, the interaction between particles (electrons, atoms, etc.) is directly dictated by their quantum mechanical (QM) state;

- the microscopic scale ($\sim 10^{-6}$ m), where phenomena related to the behavior of atoms are considered. The interaction between atoms is governed by empirical interatomic potentials, which are generally derived from

QM computations. Classic Newtonian mechanics is used to compute the displacements and rotations of atoms;

- the mesoscopic scale ($\sim 10^{-4}$ m), where phenomena related to lattice defects are considered. At this scale, the atomic degrees of freedom are not explicitly treated, and only larger scale entities (clusters of atoms, clusters of molecules, etc.) are considered. The interaction between particles is also described by classic Newtonian mechanics;

- the macroscopic scale ($\sim 10^{-2}$ m), where macroscopic phenomena which can be described by continuum mechanics are considered. At this scale, the studied physical systems are regarded as continua, whose associated behavior is described by constitutive laws.

Typically, the DMs cover the first three scales. At these scales, the length scale of interest is at the same order of magnitude as the discontinuity spacing, which makes inappropriate the application of traditional CMs. Otherwise, additional handling is required to correctly reproduce phenomena associated with discontinuities like strain localization at crack initiation. At the macroscopic scale, most of the interesting materials can be treated as continua even though they consist of discrete grains at smaller scales. CMs can therefore be used without remorse at this scale. However, it is often rewarding to model such materials as discontinuous by DMs because new knowledge can be gained about their macroscopic behavior when their microscopic mechanisms are understood. The need to model these materials as discontinuous is even more rooted when they are characterized by complex nonlinear mechanical behaviors that cannot easily be described by traditional continuum theories, e.g. anomalous behavior of silica glass [JEB 13b]. This reflects the tremendous diversity of problems to which discrete element modeling can be applied and the ever-increasing availability of DMs. Section 1.2 gives a bird's-eye view of these methods, in order to position the one

that is used in this book; the reader can refer to [DON 09, JIN 07, JEB 14] for more detail. The common feature of these methods is that the studied material is modeled by a set of discrete elements, which can be of different shape and size. These elements interact with each other by contact laws and/or cohesive bonds whose type is directly dictated by the physics of the material being modeled. Knowing forces and torques applied on the discrete elements, displacements and rotations can be computed using the Newton's second law. For practical purposes, it would be often beneficial to express these results in terms of homogeneous macroscopic variables (e.g. strains and stresses). This allows us, for example, to compare the numerical results with experimental ones. Several techniques have been developed to assess macroscopic quantities from the discrete variables (e.g. force, displacement, etc.). The most commonly used techniques are detailed in section 1.4.

1.2. Classification of discrete methods

According to the analysis scale, the DMs most commonly used in numerical simulation can be classified into three classes: quantum mechanical (or *ab initio*) methods (QMMs), atomistic methods (AMs) and mesoscopic DMs (MDMs) (Figure 1.1).

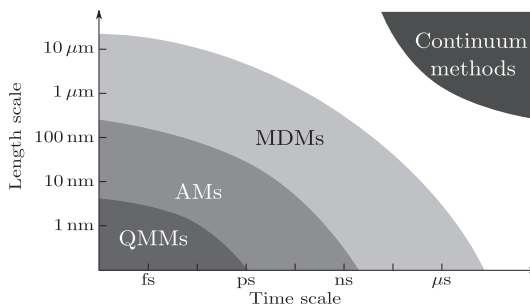


Figure 1.1. Characteristic length scales and time scales for numerical methods

1.2.1. *Quantum mechanical methods*

The QMMs are used for material simulation at the atomic scale ($\sim 10^{-9}$ m), in which the electrons are the players (Figure 1.1). The molecules are treated as collections of nuclei and electrons whose interaction is directly dictated by their QM state, without any reference to “chemical bonds”. These methods all ultimately stem from the Schrödinger equation first brought to light in 1925. The fully time-dependent form of this equation for a single particle p (e.g. electron) is expressed as:

$$\left[-\frac{\hbar}{2m^p} (\nabla^2 + \Phi(\mathbf{r}^p, t)) \right] \Psi(\mathbf{r}^p, t) = i\hbar \frac{\partial \Psi(\mathbf{r}^p, t)}{\partial t} \quad [1.1]$$

where m^p and \mathbf{r}^p are, respectively, the mass and position vector of the particle of interest, t designates the time, Φ is an external field (e.g. electrostatic potential), ∇^2 is the Laplacian, \hbar is Planck’s constant divided by 2π , i is the square root of -1 and Ψ is the wave function which characterizes the particle motion. In fact, the wave function Ψ can properly be obtained for all the particles within a system, which, for crystalline materials, is actually reduced to the primitive unit cell because of translational symmetry. However, equation [1.1] needs this function to be expressed for individual particles. To get around this, the technique most commonly used is to write the overall wave function as a product of single-particle wave functions (the Slater determinant) and then to recast the underlying Schrödinger equation in terms of these functions. Solving this equation gives the particle motions, which in turn give the molecular structure and energy among other observables, as well as information about bonding. The challenge in developing QMMs is that such an equation can be solved exactly only for few problems, e.g. one-electron system (the hydrogen atom), and approximations need to be made. The approximation commonly used is the so-called “Hartree–Fock” which consists of replacing the “correct”

description of particle (electron) motions by a picture in which the particles behave essentially as independent bodies. Several other approximations can be found in the literature. These approximations constitute the main difference between QMMs. Examples of these methods are quantum Monte Carlo (QMC) [FOU 01] and quantum chemistry (QC) [SZA 89]. These methods allow us to treat electrons explicitly and accurately, which makes them very accurate but computationally too demanding to handle more than a few tens of electrons. Other QMMs are density-functional theory (DFT) and local density approximation (LDA) [HOH 64, PAY 92]. In these approaches, the primary Schrödinger equation is expressed in terms of particle density rather than the wave functions. Although they are less accurate than QMC or QC, these methods can be readily applied to systems containing several hundred atoms for static properties. Dynamic simulations with DFT and LDA are usually limited to timescales of a few picoseconds.

Overall, the QM methods are generally very accurate since they hold out the possibility of performing simulations without need for prior tuning. However, they are extremely expensive and can only be applied on very small domains a few nanometers in size. Indeed, they deal with electrons in a system and, even if some of the electrons are ignored (as in the semi-empirical approaches), a large number of particles must still be considered.

1.2.2. Atomistic methods

The AMs are used for material simulation at the microscopic scale ($\sim 10^{-6}$ m), where atoms are the players (Figure 1.1). These methods ignore the electronic motions and compute the energy of a system as a function of the atomic positions only. This way to compute energy derives its legitimacy from the Born–Oppenheimer approximation, which postulates that the electrons adjust to the new atomic

positions much faster than the atomic nuclei. The interaction laws between particles (atoms) can be described by empirical interatomic potentials that encapsulate the effects of bonding (mediated by electrons) between them. These potentials may depend on the distance between particles, angles between bonds, angles between planes, etc. Equation [1.2] gives the general form of these potentials:

$$\begin{aligned}\Phi(\mathbf{r}1, \mathbf{r}2, \dots, \mathbf{r}N) = & \sum p \Phi_1(\mathbf{r}p) + \sum p \sum q, q > p \Phi_2(\mathbf{r}p, \mathbf{r}q) \\ & + \sum p \sum q, q > p \sum m, m > q \Phi_3(\mathbf{r}p, \mathbf{r}q, \mathbf{r}m) \\ & + \dots\end{aligned}\tag{1.2}$$

where \mathbf{r}^p is the position vector of a particle (atom) p , N is the total number of particles, Φ_1 is the one-particle part of Φ (due to external field or boundary conditions) and Φ_2 and Φ_3 are, respectively, the two-particle and three-particle parts of Φ due to interaction between particles. The interatomic potentials may include several parameters which can be obtained by calibration using experimental data or from QM calculations. When only Φ_2 parts are present, the associated Φ is called the pair potential, e.g. Hard sphere potential and Lennard–Jones potential. The Hard sphere potential (Figure 1.2a) is the simplest part (without any cohesive interaction) and is generally used in the theoretical investigation of some idealized problems:

$$\Phi(l^{pq}) = \begin{cases} \infty & \text{for } l^{pq} \leq l_0 \\ 0 & \text{for } l^{pq} > l_0 \end{cases}\tag{1.3}$$

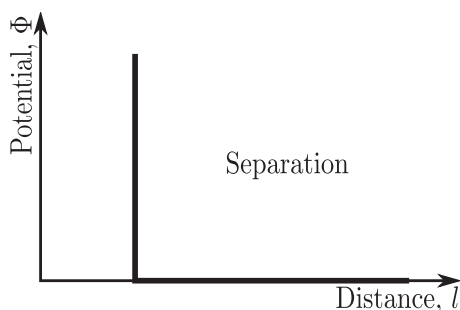
where $l^{pq} = \|\mathbf{r}^q - \mathbf{r}^p\|$ is the distance between two particles p and q and l_0 is the cutoff distance. The Lennard–Jones potential (Figure 1.2b) is more complex and more realistic to

model some physical interactions, such as the van der Waals interaction in inert gases and molecular systems:

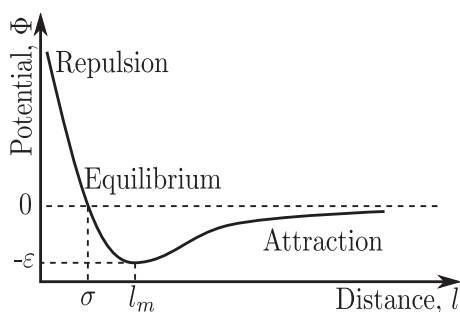
$$\Phi(l^{pq}) = 4\varepsilon \left[\left(\frac{\sigma}{l^{pq}} \right)^{12} - \left(\frac{\sigma}{l^{pq}} \right)^6 \right] = \varepsilon \left[\left(\frac{l_m}{l^{pq}} \right)^{12} - 2 \left(\frac{l_m}{l^{pq}} \right)^6 \right] \quad [1.4]$$

where ε is the depth of the potential well (the region surrounding the potential minimum), σ is the finite distance at which the interparticle potential is zero and l_m is the distance at which the potential reaches its minimum. Several papers providing the Lennard–Jones parameters for some molecular systems can be found in the literature [ASH 76, HAL 75]. The pair interatomic potentials are currently the most commonly used because of their simplicity and their relatively good ability to model several molecular systems. However, in some complex problems, more sophisticated many-body potentials (including Φ_3 and higher terms) are required to correctly reproduce the involved interaction mechanisms. Knowing the interatomic potential Φ , the loadings acting on the particles (atoms) can be obtained. Then, Newton’s second law can be applied to find the motions of these particles. This is the key idea of the AMs. Examples of these methods are molecular mechanics (statics) (MM) [HEH 03], molecular dynamics (MD) [ALD 57, ALD 59] and MC [MET 49], which are widely used in molecular simulation.

Although they are less accurate than the QMMs, the AMs are relatively inexpensive (compared to QMMs) and are able to provide insight into atomic processes involving considerably large systems of up to 10^9 atoms [ABR 02]. Nevertheless, dynamic simulation with AM methods is generally limited to timescales of a few nanoseconds, which can be crippling for the simulation of realistic mechanical problems.



(a) Hard sphere potential



(b) Lennard–Jones potential

Figure 1.2. *Examples of pair potentials*

1.2.3. Mesoscopic discrete methods

To overcome the timescale limitations of the QMMs and the AMs, another generation of DMs has been developed: MDMs. The MDM methods can be used for material simulation at the mesoscopic scale ($\sim 10^{-4}$ m), where lattice defects such as dislocations, crack propagation and other microstructural elements are the players. At this scale, the system is too small to be regarded as a continuum and too large to be simulated effectively using QMMs or AMs. More accurately, the mesoscopic scale can be defined as an intermediate scale at which the microscopic phenomena (e.g. particle motions) can be assumed in mechanical equilibrium, but cannot be described by continuum mechanics. The MDMs

can broadly be regarded as a generalization of the AMs, where more complex interaction laws are used. These interaction laws are usually derived by calibration or from phenomenological theories that encompass the effects of interactions between atoms. In MDMs, the atomic degrees of freedom are not explicitly treated and only larger-scale particles are modeled. Originally, this class of methods was developed to model movements within granular materials in rock mechanics [CUN 71]. Subsequent works have extended this class to study damage in various geometricals such as concrete [HEN 04b] and rocks [BOB 09]. More recently, attempts to apply this class of method on continuous materials (continua), such as ceramics [TAN 09] and glasses [AND 13, JEB 13b, JEB 13a, AND 12b], have emerged. In these attempts, the continuum is also modeled by an agglomerate of discrete elements (particles or nodes) which interact via bilateral cohesive links to ensure the material cohesion. Different cohesive links are tested according to the physical properties of the studied material. Figure 1.3 illustrates an example of a continuum modeled by the MDM method. As will be seen in Chapter 2, the application of MDMs methods in modeling of continua must respect certain geometric and mechanical rules.

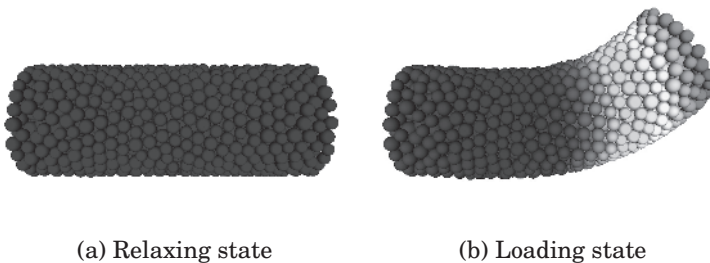


Figure 1.3. *MDM modeling of a continuum. For a color version of the figure, see www.iste.co.uk/jebahi/discrete.zip*

Nowadays, the MDMs present an alternative method to study realistic complex problems, for which continuity assumption is not valid, or problems with discontinuities that cannot easily be treated by CMs, such as cracking behavior of silica glass [AND 13, JEB 13b, JEB 13a, AND 12b]. The benefits of these methods have attracted several researchers, and consequently, several variations of MDMs have been developed. These variations can be divided into four categories as shown in Figure 1.4. The fundamental concepts of each one are briefly recalled hereafter.

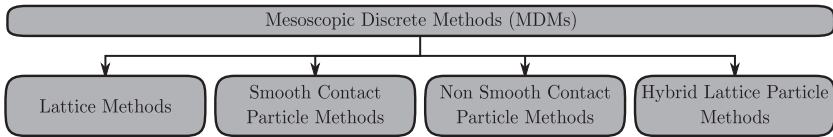


Figure 1.4. Classification of mesoscopic discrete methods (MDMs)

1.2.3.1. Lattice methods

In lattice models, a solid is modeled by a set of nodes connected with truss or beam elements [SCH 92a, SCH 92b] (Figure 1.5). Typically, nodes have neither masses nor volumes (they do not occupy volumes). Solving a mechanical problem with this class of DMs is based on the construction of a global stiffness matrix \mathbf{K} from the local connection properties. Knowing this matrix, the displacements \mathbf{u} and rotations θ at the nodes can be obtained for static analysis by solving:

$$\mathbf{K} \mathbf{X} = \mathbf{b} \quad [1.5]$$

where \mathbf{X} is the vector of the problem unknowns which includes both displacements and rotations of all the nodes and \mathbf{b} is the loading vector which includes forces and torques in the beams. Both regular and irregular lattices were studied. Originally, the lattice models were used to represent elastic continuum; the equivalence was established for both

truss [HRE 41] and beam [SCH 96] elements. Later on, obvious enhancements, such as brittle beam failure, were introduced. Lattice models nicely show the emergence of relatively complex structural behaviors, although fairly simple formulas are used to describe the governing local processes.

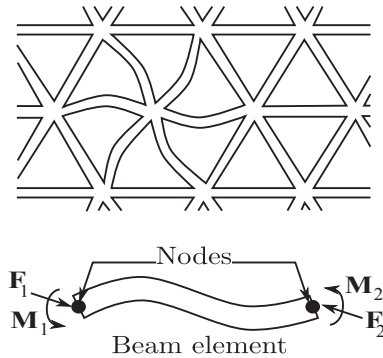


Figure 1.5. 2D regular triangular lattice of beams
(inspired by [SCH 92a])

Lattice models have shown a great ability to model fracture in continuous materials. Schlangen *et al.* [SCH 97] pointed out that using beam elements (forces and torques are considered), the crack pattern is quite close to the experimentally observed pattern. The same authors [SCH 97] emphasized the importance of the beam torques, without which the crack behavior may be entirely unacceptable. The major drawback of these models is that the nodes do not have volumes, which can cause numerical problems related to crack closure in postfracture stage. To circumvent this problem, Ibrahimbegovic *et al.* [IBR 03] have proposed to associate fictitious equivalent volumes with the nodes, based on the spatial Voronoï decomposition. However, this solution is generally time-consuming, especially in the case of large three-dimensional (3D) problems.

1.2.3.2. *Smooth contact particle methods*

This class of methods is very close to the first discrete approach proposed in the literature by Cundall and Strack [CUN 71, CUN 79]: distinct (discrete) element method (DEM). Contrary to lattice models, particle models consider elements with masses and volumes in interaction through contact laws. These elements often have a disk shape (in two-dimensional (2D)) or spherical shape (in 3D): only one parameter (the radius) is required to determine the geometry of elements and there is only one possible contact easily detectable between them. Consequently, computer memory requirements and processing time are minimized with these element shapes, even when a relatively large number of elements are used. Nevertheless, discs and spheres can roll or rotate easily. This does not reflect the expected behavior for several materials, for example, in the case of large shear processes. To solve this problem, more complex shapes such as ellipses [TIN 93], ellipsoids [LIN 97], polygons [ISS 92] and polyhedra [CUN 88] were proposed in the literature to provide more flexibility for element characterization in particle models.

Basically, the associated algorithm involves two stages. In the first stage, interaction forces are computed when elements slightly interpenetrate each other. This force-interpenetration formulation is generally referred to as a “smooth contact” method or “force–displacement” method. Actually, the interpenetration between discrete elements, which makes no mechanical sense, represents the relative deformation of the surface layers. In the second stage, Newton’s second law is applied to determine the acceleration of each element, which is then integrated, using “*dynamic explicit*” schemes, to find the new velocities and positions of elements. This process is repeated until the simulation is achieved.

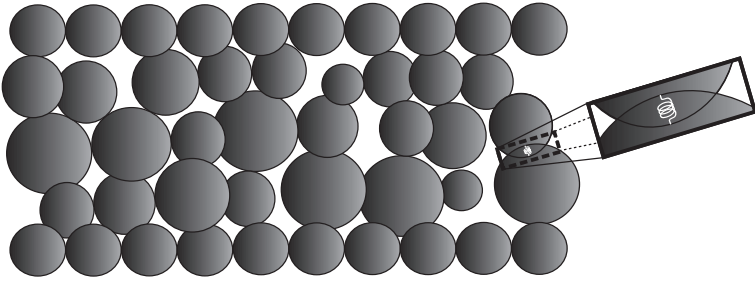


Figure 1.6. *2D smooth contact particle model*

1.2.3.3. *Non-smooth contact particle models*

Despite the great success of the smooth contact particle models to simulate a wide variety of complex systems, there are cases for which they are less appropriate:

- in systems where the typical duration of a collision is much shorter than the mean time between successive collisions of a particle. Therefore, the pairwise collisions of particles may be considered as instantaneous events;
- in systems where the contact laws between particles cannot easily be determined as a function of the relative position, velocity and orientation; however, information about postcollision velocities is accessible from the precollision conditions (e.g. by using experimental techniques);
- in systems where the particles are very rarely in contact with more than one other particle.

To allow a better investigation of such systems, another class of DMs has been developed. This class provides an alternative approach based on a “non-smooth” formulation of mutual exclusion and dry friction between elements [JEA 99, LUD 96, MOR 94]. It introduces the notion of non-smooth (irregular) contact between elements which is, at present, the subject of several studies. Interpenetration between elements is prevented: no elastic contact laws are used between them.

Mainly, two classes of numerical integrators exist for non-smooth contact methods; both of them are of the “*dynamic implicit*” type: the event-driven integrators, also referred to as the event-driven method (EDM) [LUD 96], and the time-stepping integrators, also referred to as the contact dynamics method (CDM) [JEA 99, MOR 94]. In EDM, a collision or “event” occurs when two rigid elements touch each other and the postcollisional and angular velocities are prescribed by a collision operator [RAP 80]. Despite being very accurate, the event-driven integrators treat only one force at a time. Therefore, they are not well adapted for problems with many simultaneous contacts, as often encountered in mechanics. To overcome this limitation, Jean and Moreau [JEA 99, MOR 88] have developed the CDM which has a specialized numerical scheme for problems with many contacts. The governing equations are expressed as differential inclusions (multivalued differential equations) and the accelerations are replaced by velocity jumps. In the generic CDM algorithm, an iterative process is used to compute forces and velocities. This process consists of solving a single contact problem with all other contacts kept constant, and iteratively updating the forces until a convergence criterion is fulfilled. Two basic kinematic constraints are used between elements in the CDM formulation:

- the *Signorini conditions* which state that the normal force f_n is repulsive when the elements are in contact (distance between them is zero), and $f_n = 0$ otherwise. To deal with persistent contacts, f_n is reset to zero when no relative velocity exists between elements in contact;
- *Coulomb’s friction law*, which relates the sliding particle velocities and the friction forces f_t .

These kinematic constraints can also be complemented by a “*rolling friction*” constraint which introduces a moment resistance [BRA 02]. Within the CDM, the time resolution is much larger than the collision characteristic time (unlike in

the case of smooth contact approaches). Therefore, the time step represents a unit of time during which collisions can occur, causing velocity jumps. Although CDM has successfully been used for several geomechanical problems [DON 09], it is much more difficult to implement than the DMs based on smooth contact. Also, the prediction of the contact forces and particle velocities in the following time step from the current configuration is very problematic and is currently the subject of several studies.

The non-smooth contact models are generally used to study quasi-static problems or problems with relatively low dynamic effects. This class of methods is perfectly suitable to study mechanical problems of granular mechanics. However, in the case of continuous media, the use of models based on regular or “smooth” interaction laws seems to be advantageous since the elasticity is naturally taken into account by these interaction laws.

1.2.3.4. *Hybrid lattice-particle models*

As seen earlier, the features and advantages of the lattice and particle models are largely complementary. Indeed, the particle methods cannot correctly model a continuum using a simple disk of spherical elements, especially when significant shear effects are involved. This problem can be solved using cohesive beams between elements, such as in lattice models. On the other hand, particle methods can correctly deal with crack closure in postfracture stage, since elements have their own volumes. However, additional treatment must be made to simulate this phenomenon by using lattice models. Therefore, it would be beneficial to combine these models, in order to strengthen their advantages and overcome their drawbacks. This idea has attracted a strong research effort which has given rise to the class of hybrid lattice-particle methods. This class merges the main features of the combined models, i.e. by considering sphere elements connected with cohesive beams [GRI 01] (Figure 1.7).

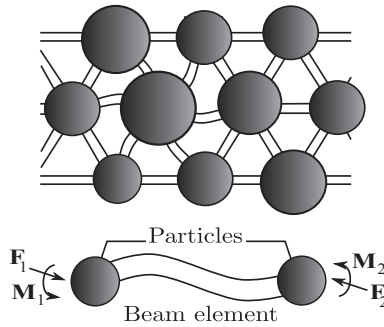


Figure 1.7. *2D hybrid lattice-particle model*

1.3. Discrete element method for continuous materials

As seen in the previous section, the DMs are classified into three classes: QMMs, AMs and MDMs. The first two classes are adapted for very fine-scale problems for which continuum description is not possible. Application of these classes to study continuous materials whose scale of interest is much greater than the interatomic distance is extremely time-consuming or even crippling. The MDMs are used to study the problems at the mesoscopic scale which is the scale of interest for most of the complex phenomena that are encountered in continuum simulation, but cannot correctly be treated by CMs. Compared to QMMs and AMs, these methods are relatively inexpensive and seem to be the most adapted to simulate continuous materials. Mainly, four categories of MDMs can be distinguished. The category of non-smooth contact methods is based on a non-smooth formulation between particles. This formulation can be perfectly adapted for granular materials; however, it is inappropriate to study continuous materials. In effect, the use of models based on regular or “smooth” interaction laws seems to be advantageous for these materials since their mechanical behavior can naturally be taken into account by the smooth interaction laws. Except for the non-smooth contact methods, all MDM categories present this feature (of

smooth interaction between particles) and seem *a priori* candidates to model continuous materials. Among them, the category of hybrid lattice-particle methods has practically all the advantages of the MDM categories with regard to continuum simulation, while alleviating their drawbacks. The use of a DM in this category to model continua is thereby justified. Specifically, this book focuses on the variation of DMs recently developed by André *et al.* [AND 12b, AND 13, JEB 13b, TER 13, JEB 13a]. This method models a continuum by a set of spherical particles linked by 3D cohesive beams. The main specificities and features of this method will be detailed later.

1.4. Discrete-continuum transition: macroscopic variables

In the framework of discrete element modeling, results of a mechanical problem are given in terms of forces and torques acting on particles, and their corresponding displacements and rotations. However, in order to compare these results with macroscopic experiments or theories, it is useful to assess macroscopic quantities from these results. This is the subject of several works which aim to establish a correspondence with continuum theories by computing macroscopic tensorial quantities, e.g. stress tensor σ and strain tensor ε , as well as other scalar properties, e.g. bulk and shear moduli [GOD 86, KRU 96, LIA 97]. These macroscopic quantities can even be applied to enrich some criteria used in discrete element modeling. As will be shown in Chapter 4, fracture criteria based on a stress tensor allow us to reproduce the cracking mechanisms much better than the traditional criteria based on the forces or displacements. The major challenge in obtaining these quantities is that, in some variations of DMs, the particles have additional degrees of freedom (rotations) which are not taken into account in classical continuum theories. To account for rotation effects, it is necessary to develop a consistent size-dependent

continuum theory able to account for the microstructure of materials. This theory must span many scales and, of course, reduce to classical theories for the macroscopic scale. More accurately, new length-related measures of deformation, such as the curvature tensor, are needed in a more complete continuum theory. As a result, this theory also requires us to introduce the notion of couple stress which was originally proposed by Voigt in 1887 [VOI 87]. Several attempts have been developed in the literature to establish such a theory [TOU 62, CHE 01, LEO 02, HAD 11, COS 09]. However, these attempts, with their numerous difficulties, fall far short of providing a solid formulation workable in practice [ERI 68, MIN 62, HAD 11].

In the remainder of this section, approaches used to compute stress and strain tensors will be briefly reviewed, while remaining within the framework of classic continuum theories. The contribution of couple stress will then be ignored in this review. Furthermore, the phenomena related to the kinematics of the particles and having no equivalent in continuum will not be considered. This does not mean ignoring the particle rotations, only phenomena associated with no dissipated or stocked energy are ignored, e.g. loss contact or rolling without sliding. According to several papers [CAI 95, MOR 97, AND 13, BAG 06, CAM 09], these approaches lead in a first approximation to an acceptable estimate of these tensors. For the sake of clarity, unless there is a need for index form, equations in the following will be given in matrix form. Moreover, tensors will be replaced by their corresponding matrices in the equations.

1.4.1. *Stress tensor for discrete systems*

Within the framework of classic continuum theories, the most commonly used definition of stress in DMs is the virial stress. This stress, also called system-level stress, is based on a generalization of the virial theorem of Clausius developed

in 1870 for gas pressure. In the original definition [MCL 74, TSA 79, SWE 83], the average virial stress over a volume V around a particle p is given by:

$$\bar{\Pi} = \frac{1}{V} \left(-m^p \dot{\mathbf{u}}^p \otimes \dot{\mathbf{u}}^p + \frac{1}{2} \sum_{q \neq p} \mathbf{l}^{pq} \otimes \mathbf{f}^{pq} \right) \quad [1.6]$$

where m^p is the mass of p , $\dot{\mathbf{u}}^p$ is the velocity of p (material time derivative of the displacement \mathbf{u}^p , $\dot{\mathbf{u}}^p = d\mathbf{u}^p/dt$), $\mathbf{l}^{pq} = \mathbf{r}^q - \mathbf{r}^p$ is the vector linking the centers of particles p and q , \mathbf{r}^p is the position vector of p , \mathbf{f}^{pq} is the force applied on p by particle q , “ \otimes ” denotes the tensor product and the summation runs over all the particles in V . The sign convention for solid mechanics is used in the virial stress relation [1.6], i.e. the stress is negative in compression and positive in extension. This relation includes two parts. The first part depends on the mass and velocity (or in some versions the fluctuations of velocity) of the particles, reflecting that the mass transfer through a fixed spatial surface causes mechanical stress on this surface. The second part depends on the interparticle forces and particle positions, providing a continuum measure for the internal mechanical interactions between particles.

The virial stress as defined in [1.6] has widely been used in the past to compute an equivalent to Cauchy stress in discrete systems. Recently, Zhou [ZHO 03] has demonstrated that, contrary to what was believed by some investigators, this quantity is not a measure for the mechanical forces between material points and cannot be regarded as a measure of mechanical stress in any sense. The lack of physical significance is both at the microscopic level (particle level) and macroscopic level (system level). This author has shown that only the second part of the virial stress can be identified with the Cauchy stress. The details of the proof can

be found in [ZHO 03]. Therefore, the average stress in a region of volume V as given by Zhou is:

$$\bar{\sigma} = \frac{1}{2V} \sum_p \sum_{q \neq p} \mathbf{l}^{pq} \otimes \mathbf{f}^{pq} \quad [1.7]$$

Originally, expressions [1.6] and [1.7] were developed for MD where the interparticle forces are derived from a functional Φ (e.g. Lennard–Jones potential [1.4]) as follows:

$$\mathbf{f}^{pq} = \frac{\partial \Phi(\mathbf{l}^{pq})}{\partial l^{pq}} \frac{\mathbf{l}^{pq}}{l^{pq}} \quad [1.8]$$

where $l^{pq} = \|\mathbf{l}^{pq}\|$ represents the distance between particles p and q . In this instance, expressions [1.6] and [1.7] lead to symmetric tensors. However, this cannot be generalized to all DMs. To analyze the symmetry of the stress tensor [1.7] for the general case, the approach proposed by Chapuis [CHA 76] for quasi-static analysis can be used.

For quasi-static study, the resultant torque on a particle p must vanish:

$$\sum_{q \neq p} \mathbf{l}^{pq} \wedge \mathbf{f}^{pq} = 0 \quad [1.9]$$

which is equivalent to:

$$\sum_{q \neq p} l_i^{pq} f_j^{pq} - l_j^{pq} f_i^{pq} = 0, \quad \forall i, j \in [1..3] \quad [1.10]$$

Therefore,

$$\sum_{q \neq p} \mathbf{l}^{pq} \otimes \mathbf{f}^{pq} = \sum_{q \neq p} \mathbf{f}^{pq} \otimes \mathbf{l}^{pq} \quad [1.11]$$

If the volume V , in which the stress tensor is computed, includes all the particles of the studied system (i.e. the volume

boundary does not cut any particle), equation [1.9] is true for each of these particles. Therefore, the following relation can be obtained:

$$\sum_p \sum_{q \neq p} \mathbf{l}^{pq} \otimes \mathbf{f}^{pq} = \sum_p \sum_{q \neq p} \mathbf{f}^{pq} \otimes \mathbf{l}^{pq} \quad [1.12]$$

which proves the symmetry of the stress tensor given by [1.7]. However, if some particles are cut by the boundary of the considered volume, equation [1.9] is not valid for these particles. In this case, the symmetry of the stress tensor [1.7] is not guaranteed. However, if the volume V is large enough, the number of particles cut by the volume boundary is small with respect to the total number of particles in V . The associated stress tensor can therefore be considered as symmetric [CAI 95, MOR 97].

For dynamic study, the above analysis can also be followed when the particle forces are symmetrically applied around each particle center (as in regular assemblies). In this case, no particle torques are induced on the particles, and then equation [1.9] remains valid. If the particle forces are not highly unsymmetrical, the corresponding stress tensor can be assumed to be symmetric. Otherwise, the symmetric part of [1.7] can be used to compute an approximated stress tensor in discrete systems [AND 13, JEB 13b]:

$$\bar{\boldsymbol{\sigma}} = \frac{1}{2V} \sum_p \sum_{q \neq p} \frac{1}{2} (\mathbf{l}^{pq} \otimes \mathbf{f}^{pq} + \mathbf{f}^{pq} \otimes \mathbf{l}^{pq}) \quad [1.13]$$

1.4.2. Strain tensor for discrete systems

The micromechanical interpretation of a strain tensor in discrete systems has been the subject of strong scientific interest in recent years. Consequently, several approaches have been proposed to this end. All these approaches are based on the assumption of small displacements of the

particles. Most of them are derived either from equivalent continuum computations or using best-fit methods. A brief review of the approaches commonly used is given hereafter; the reader is referred to [BAG 06, CAM 09] for more details. Only 3D domains are considered in this review, but almost all the reviewed approaches can also be used for 2D analysis. Let Ω_D denote the discrete region (made up of N particles) in which the strain tensor would be computed.

1.4.2.1. *Equivalent continuum strains*

These microstructural strains are based on the equivalent continuum technique. The discrete region Ω_D is replaced by an equivalent continuous domain, to which a displacement field is assigned such that the displacements of the continuum nodes (associated with the equivalent continuous domain) are equal to those of the particle centers. The strain tensor can then be determined from the gradient of this field, and expressed in terms of the particle displacements and the geometrical characteristics of the discrete model. Several approaches based on this technique can be found in the literature [BAG 93, BAG 96, KUH 99, CAM 00, KRU 03, KRU 96], some of which are studied and compared in [CAM 09, BAG 06]. The main difference between them lies in the way in which the equivalent continuum is defined. One particular approach is that suggested by Bagi [BAG 93, BAG 96], which can be regarded as a generalization of the first approach developed by Rothenburg in his PhD dissertation in 1980 for 2D analysis [ROT 80]. This approach is valid for 2D and 3D systems with arbitrary convex shape. Only particle displacements are considered in such an approach (particle rotations are ignored). The continuous domain is constructed from the discrete system using a kind of “space cell”, which is defined as tetrahedra (triangles in 2D) formed by the centers of neighboring (but not necessary touching) particles (Figure 1.8). The displacement field associated with this continuum is defined using a linear

interpolation of nodal displacements, which are, by definition, the same that the particle displacements.

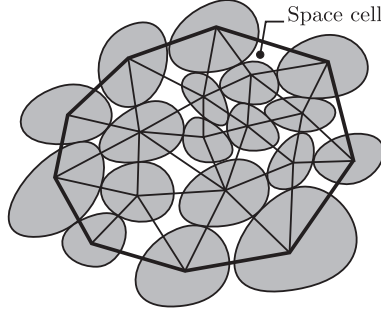


Figure 1.8. Space cells (inspired by [BAG 06])

Within a cell c , this displacement field is continuously differentiable, and its gradient is constant in this cell. Let $\mathbf{e}^c = \nabla \mathbf{u}$ denote the displacement gradient tensor in the cell c . The volume average of this tensor over the cell c can be expressed using a surface integral as follows:

$$\bar{\mathbf{e}}^c = \frac{1}{V^c} \oint_{S^c} \mathbf{u} \otimes \mathbf{n} ds \quad [1.14]$$

where V^c and S^c are, respectively, the volume and boundary surface of the cell c , and \mathbf{n} is the outward unit normal vector of S^c . Using [1.14], the volume average of the displacement gradient tensor over the whole continuum domain associated with Ω_D is given by:

$$\bar{\mathbf{e}} = \frac{1}{V} \sum_c V^c \bar{\mathbf{e}}^c \quad [1.15]$$

where $V = \sum_c V^c$ is the volume of the whole continuum associated with Ω_D . To compute [1.15], Bagi [BAG 95, BAG 96] has introduced a new vector \mathbf{d}^{pq} associated with the particle interactions pq (between particles p and q).

This vector is called the complementary area vector, and its derivation is detailed in [BAG 95, BAG 96]. It can be interpreted as the dual of the branch vector l^{pq} pointing from the center of the particle p to the center of the particle q , in the sense that the total volume of the studied domain is determined by summing the scalar products of these vectors over the total number of particle interactions pq :

$$V = \frac{1}{3} \sum_{pq} \mathbf{d}^{pq} \cdot l^{pq} \quad [1.16]$$

Using the complementary area vector \mathbf{d}^{pq} , equation [1.15] can be rewritten as:

$$\bar{\mathbf{e}} = \frac{1}{V} \sum_{pq} \mathbf{u}^{pq} \otimes \mathbf{d}^{pq} \quad [1.17]$$

where $\mathbf{u}^{pq} = \mathbf{u}^q - \mathbf{u}^p$ is the relative displacement of the centers of particles p and q . The details of the proof can be found in [BAG 95, BAG 96]. The symmetric part of the tensor $\bar{\mathbf{e}}$ defines the average strain tensor $\bar{\boldsymbol{\varepsilon}}$ in V :

$$\bar{\boldsymbol{\varepsilon}} = \frac{1}{2} (\bar{\mathbf{e}} + {}^t\bar{\mathbf{e}}) \quad [1.18]$$

Several papers studying the Bagi approach can be found in the literature [BAG 06, CAM 09]. These papers conclude that this approach generally gives a good estimate of the strain tensor at the structure scale.

1.4.2.2. *Best-fit strains*

These microstructural strains are based on the best-fit technique (e.g. using the least squares method). They consist of finding the displacement gradient tensor which gives the smallest deviation from characteristic displacements of the particles in Ω_D (the discrete region in which the strain tensor would be computed). Several best-fit approaches have been proposed in the literature [CUN 79, LIA 97, CAM 00], all of

which are valid for 2D and 3D analyses. The main difference between these approaches lies in the way in which the characteristic displacements are defined, e.g. the relative displacements of the particle centers, the relative displacements at the contacts, etc. Among the first best-fit strains is the Cundall strain [CUN 79], which is widely used in the discrete element modeling and is even implemented in several well-known software packages (e.g. PFC, TURBAL, etc.). This microstructural strain is valid for particles with arbitrary shape. The approach used to obtain this strain is detailed hereafter. It should be noted that only displacements of the particle centers (particle rotations are ignored) are considered in this approach.

Let \mathbf{x}^p and \mathbf{u}^p be the initial position vector and displacement vector of a particle p . In the approach of Cundall, the space variables are expressed in a framework whose origin o is located at the average position of the particle centers belonging to Ω_D :

$$\mathbf{x}^o = \frac{1}{N} \sum_p \mathbf{x}^p \quad [1.19]$$

where N is the total number of particles in Ω_D . The displacement of the Cundall framework is defined as the average displacement of the particle centers in Ω_D :

$$\mathbf{u}^o = \frac{1}{N} \sum_p \mathbf{u}^p \quad [1.20]$$

Therefore, the vectors \mathbf{x}^p and \mathbf{u}^p are, respectively, replaced by \mathbf{x}^{op} and \mathbf{u}^{op} . The vector \mathbf{x}^{op} represents the relative position of individual particles with respect to \mathbf{x}^o :

$$\mathbf{x}^{op} = \mathbf{x}^p - \mathbf{x}^o \quad [1.21]$$

The vector \mathbf{u}^{op} represents the relative displacement of individual particles with respect to \mathbf{u}^o :

$$\mathbf{u}^{op} = \mathbf{u}^p - \mathbf{u}^o \quad [1.22]$$

Assuming that the studied assembly deforms such that every particle displacement exactly corresponds to a uniform displacement gradient tensor $\bar{\mathbf{e}}$ (i.e. the strain tensor is assumed to be constant in Ω_D), equation [1.22] can be rewritten as:

$$\mathbf{u}^{op} = \bar{\mathbf{e}} \mathbf{x}^{op} \quad [1.23]$$

because particle displacements are assumed to be small. Therefore, the Cundall approach consists of finding the tensor $\bar{\mathbf{e}}$ that gives the best fit to the relative particle displacements [1.23]. Using the least squares method, the problem is reduced to finding the optimum $\bar{\mathbf{e}}$ that minimizes S :

$$S = \sum_p \|\mathbf{u}^{op} - \bar{\mathbf{e}} \mathbf{x}^{op}\|^2 \quad [1.24]$$

where “ $\|\cdot\|$ ” denotes the Euclidean norm. This last relation [1.24] can be rewritten in index form (using the Einstein summation convention) as follows:

$$S = \sum_p \left(u_i^{op} - \bar{e}_{ij} x_j^{op} \right)^2, \quad i, j \in [1..3] \quad [1.25]$$

The corresponding mathematical problem is: find $\bar{\mathbf{e}}$ such that:

$$\forall i, j \in [1..3], \quad \frac{\partial S}{\partial \bar{e}_{ij}} = 0 \quad [1.26]$$

which can be rewritten in matrix form as:

$$\mathbf{A} \bar{\mathbf{e}} = \mathbf{B} \quad [1.27]$$

where the matrices \mathbf{A} and \mathbf{B} are given by:

$$\mathbf{A} = \sum_p \mathbf{x}^{op} \otimes \mathbf{x}^{op}, \quad \mathbf{B} = \sum_p \mathbf{x}^{op} \otimes \mathbf{u}^{op} \quad [1.28]$$

As demonstrated by Bagi [BAG 05], the coefficient matrix \mathbf{A} is positive-definite if and only if $n \geq 4$ and there exist at least four particles whose centers are not in the same plane. This is the necessary and sufficient condition for existence of the inverse coefficient matrix \mathbf{A}^{-1} , and then the existence of the Cundall strain in 3D. If \mathbf{A}^{-1} exists, the best-fit displacement gradient tensor is given by:

$$\bar{\mathbf{e}} = {}^t(\mathbf{A}^{-1} \mathbf{B}) \quad [1.29]$$

The Cundall strain is none other than the symmetric part of [1.29]. Based on [BAG 06, CAM 09], this microstructural strain gives relatively good results, in agreement with strain measures at the structure level.

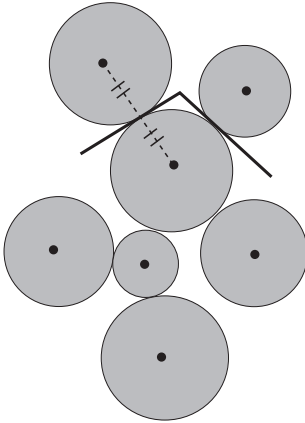
1.4.2.3. Satake strain

Contrary to the Bagi and Cundall approaches, the Satake approach [SAT 04] takes into account both displacements and rotations of the particles. Such an approach shares some features with the equivalent continuum ones. Indeed, it is based on a tessellation system (space cells). However, no displacement field assigned to these cells is required, and then no cell deformations are analyzed (unlike in equivalent continuum approaches). This approach is valid for assemblies of disk or spherical particles, as in hybrid lattice-particle methods, which is of particular interest with regard to the subject of this book.

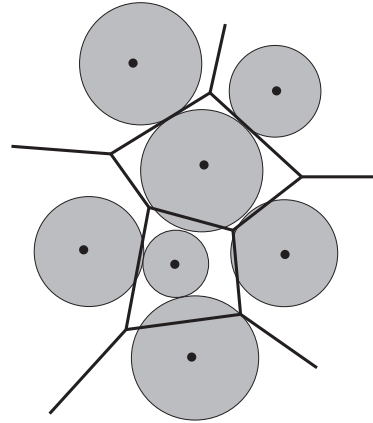
The geometrical background of the Satake strain is constructed using the generalized Dirichlet tessellation (which is also known as the Voronoï diagram) [ASH 86], whose 2D illustration is given by Figure 1.9. This tessellation

is unique for a given set of particles N , and it fills the convex hull of the particles. An individual Dirichlet cell (Voronoi cell) associated with a particle p is defined by:

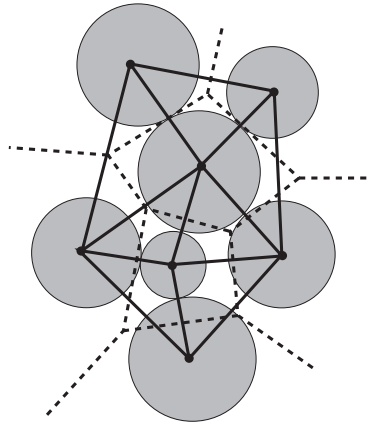
$$T_p = \{\mathbf{x} \mid \|\mathbf{x} - \mathbf{x}_p\| < \|\mathbf{x} - \mathbf{x}_q\|, \forall p \neq q\} \quad [1.30]$$



(a) Construction of generalized Dirichlet tessellation



(b) Generalized Dirichlet tessellation



(c) Delaunay tessellation

Figure 1.9. Geometric construction of the generalized Dirichlet tessellation and the associated Delaunay tessellation for a set of particles in 2D

Using [1.30], the generalized Dirichlet tessellation P can be obtained:

$$P = \{T_p | p \in [1..N]\} \quad [1.31]$$

After construction of P , the Delaunay tessellation (Figure 1.9c) can be formed by the branches connecting the centers of the particles which have a common face in P . This allows us to define the neighboring particles: every two particles p and q linked by a Delaunay branch are considered as neighbors. Then, the contact cells can be defined, based on the generalized Dirichlet tessellation and the associated Delaunay network, such that one contact cell is defined per pair of neighboring particles. The contact cell associated with the pair of particles (p and q) will be denoted by pq . For each pq , two vectors are introduced: branch vector l^{pq} linking the centers of the neighboring particles p and q and the dual branch vector d^{pq} , whose direction is perpendicular to the Dirichlet face between these particle and magnitude is equal to the area of this face. The volume of this cell can be obtained using these two vectors as:

$$V^{pq} = \frac{1}{3} \mathbf{d}^{pq} \cdot l^{pq} \quad [1.32]$$

After long and complicated calculations which can be found in [SAT 04], Satake has shown that the volume average of the displacement gradient tensor over the whole considered domain is defined by:

$$\bar{\mathbf{e}} = \frac{1}{V} \sum_{pq} \mathbf{c}^{pq} \otimes \mathbf{d}^{pq} \quad [1.33]$$

where $V = \sum_{pq} V^{pq}$ is the volume of the whole domain and \mathbf{c}^{pq} is the contact deformation defined as the relative displacement, between two particles p and q , expressed at the contact point c .

This quantity can be determined using particle displacements (\mathbf{u}^p and \mathbf{u}^q) and the particle rotations ($\boldsymbol{\theta}^p$ and $\boldsymbol{\theta}^q$) as follows:

$$\mathbf{c}^{pq} = \{\mathbf{u}^q\}_c - \{\mathbf{u}^p\}_c = (\mathbf{u}^q + \boldsymbol{\theta}^q \wedge \mathbf{r}^{cq}) - (\mathbf{u}^p + \boldsymbol{\theta}^p \wedge \mathbf{r}^{cp}) \quad [1.34]$$

where $\{\mathbf{u}^p\}_c$ is the displacement of the particle p expressed at the contact point c , \mathbf{u}^p is the displacement of the center of the particle p , $\boldsymbol{\theta}^p$ is the rotation of a particle p , \mathbf{r}^{cp} is a vector pointing from the center of the particle p to the contact (boundary) point c and “ \wedge ” denotes the vector product. The symmetric part of $\bar{\mathbf{e}}$ represents the Satake strain.

As can be seen from [1.17] and [1.33], the Satake strain expression is similar to that obtained by Bagi. One difference is that the dual branch vector is used in place of the so-called complementary area vector in the Bagi definition. This is due to a difference in the definition of the geometrical background of two microstructural strains. The generalized Dirichlet tessellation is used to obtain the Satake strain, which allows us to properly define a geometric background that takes into account the particle size. This makes the geometrical explanation more simple and clearer so that a systematic analysis becomes easy both in 2D and 3D analyses. Another difference between the strain definitions is that the Bagi definition is based upon relative displacements between the particle centers, whereas relative displacements at the contact points are considered for the Satake definition. This allows us to take into consideration the particle rotations in the computation of the microstructural strain. Numerical comparison of these two definitions of microstructural strain shows that they give similar results, which are in good agreement with the strain measured at the structure level [BAG 06, CAM 09]. This can reflect that the contribution of the particle rotations is not of major importance in the computation of the strain tensor.

1.5. Conclusion

This chapter provides a brief review of discrete element modeling. A classification of the DMs most commonly used to model physical systems is given, in order to place the DEM proposed in this book. Depending on the analysis scale, three classes can be distinguished: QMMs, AMs and MDMs. The first two classes are extremely time-consuming and can be applied only to simulate very small-scale problems. The MDMs are used to simulate problems at the mesoscopic scale, which is the scale of interest of most of the complex phenomena encountered in continuum modeling (i.e. by using CMs). Therefore, this class provides an alternative method to model such phenomena. MDM methods are generally made up of four categories: lattice methods, smooth contact particle methods, non-smooth contact particle methods and hybrid lattice-particle methods. The non-smooth contact particle methods are based on the non-smooth formulation between particles. Such a category is rather adapted for granular materials. The other categories are based on the smooth particle interactions, and then come forward as candidates to model continuous problems. Indeed, the mechanical behavior of these materials can naturally be taken into account by such interactions. In particular, the category of hybrid lattice-particle methods has practically all the advantages of the MDM methods with regard to modeling of continuous materials. This is why a hybrid lattice-particle method is chosen to model continua in this book. The main features of this method will be detailed in the next chapter. The results of such a method and the DMs, in general, are given in terms of discrete particle loadings (forces and torques) and their corresponding particle motions (displacements and rotations). These results are strongly heterogeneous: their size and magnitude may significantly vary from particle to particle. Therefore, they cannot be estimated as continuously differentiable fields. Establishing a link between particle-level results and structure-level stresses and strains

is important to interpret these results from a macroscopic point of view. The second part of this chapter gives some analytical and numerical techniques used to bridge these levels. As will be seen in Chapter 4, these techniques are also useful to enrich the criteria applied in discrete element modeling.